nature COMMUNICATIONS

ARTICLE

Received 19 Jul 2014 | Accepted 21 Nov 2014 | Published 14 Jan 2015

DOI: 10.1038/ncomms6923 OPEN

Size dependence of phase transitions in aerosol nanoparticles

Yafang Cheng[1], Hang Su[1], Thomas Koop[2], Eugene Mikhailov[3] & Ulrich Pöschl[1]

Phase transitions of nanoparticles are of fundamental importance in atmospheric sciences, but current understanding is insufficient to explain observations at the nano-scale. In particular, discrepancies exist between observations and model predictions of deliquescence and efflorescence transitions and the hygroscopic growth of salt nanoparticles. Here we show that these discrepancies can be resolved by consideration of particle size effects with consistent thermodynamic data. We present a new method for the determination of water and solute activities and interfacial energies in highly supersaturated aqueous solution droplets (Differential Köhler Analysis). Our analysis reveals that particle size can strongly alter the characteristic concentration of phase separation in mixed systems, resembling the influence of temperature. Owing to similar effects, atmospheric secondary organic aerosol particles at room temperature are expected to be always liquid at diameters below ~20 nm. We thus propose and demonstrate that particle size should be included as an additional dimension in the equilibrium phase diagram of aerosol nanoparticles.

[1] Multiphase Chemistry Department, Max Planck Institute for Chemistry, 55128 Mainz, Germany. [2] Faculty of Chemistry, Bielefeld University, 33615 Bielefeld, Germany. [3] Institute of Physics, St. Petersburg State University, 198904 St. Petersburg, Russia. Correspondence and requests for materials should be addressed to H.S. (email: h.su@mpic.de) or to Y.C. (email: yafang.cheng@mpic.de) or to U.P. (email: u.poschl@mpic.de).

The phase state of aerosol particles is a key determinant of their physico-chemical interactions, climate and health effects[1–4]. Chemical composition, relative humidity and temperature have been recognized as the main factors controlling aerosol phase state[1,2,5], but they are insufficient to explain observations for nanometer-sized particles, even for well-studied inorganic reference substances[3,6–10], such as ammonium sulphate (AS).

Progress in resolving these discrepancies has been hampered by a lack of reliable thermodynamic data, such as water and solute activities and interfacial energies. This lack of data exists because nanodroplets can become more highly supersaturated (with respect to a crystal) when compared with bulk solution samples, but traditional measurement techniques and data, especially the liquid-vapour interfacial energy (σ_{lv}, also called surface tension), are mostly limited to sub-saturated and saturated solutions. The existing measurement techniques for σ_{lv} often require touching the solution by needles or other intermediates, such as a plate or capillary tube[11]. Solute crystallization induced by heterogeneous nucleation can take place in supersaturated solution on the contact surface, which makes the precise measurements difficult. Measurement of σ_{lv} using the vibration modes of a magnetically levitated drop could avoid the contact but is limited to supermicrometre particles owning to the stability in the magnetic trap[12]. Measurements of water activities (a_w) have been extended to supersaturated range by Electrodynamic Balance (EDB) methods[13,14] (for example, up to $\sim 30\,mol\,kg^{-1}$ for AS), but it is not applicable for the nanosize range either.

To overcome these limitations, we develop a new method for the determination of these specific thermodynamic parameters, closing the gap between experimental and modelled results. Further analysis reveals that particle size can strongly alter the phase separation process in mixed systems. We thus propose and demonstrate that particle size should be included as an additional dimension in the equilibrium phase diagram of aerosol nanoparticles.

Results

Thermodynamic properties of supersaturated nanodroplets. According to theoretical predictions, AS nanoparticles are expected to show a strong size dependence of deliquescence relative humidity (DRH) similar to sodium chloride (NaCl), with differences up to ~10% RH between particles with dry diameters of 6 and 60 nm (refs 6,8; Fig. 1a). Experimental data, however, reveal a much weaker size dependence for AS, that is, similar DRH values for 6-nm and 60-nm particles[9] (Fig. 1b). Moreover, model calculations based on previously available thermodynamic data agree reasonably well with the hygroscopic growth observed for both 60-nm and 6-nm NaCl particles and also for 60-nm AS particles, but deviate strongly for 6-nm AS particles as shown in Fig. 1a,b. Further investigations of these discrepancies, however, were impeded by a lack of reliable thermodynamic data.

In this study, a new method, termed Differential Köhler Analysis (DKA), is developed for the determination of thermodynamic properties from hygroscopic growth measurement data of aerosolized nanodroplets. Differential application of the classical Köhler equation to aerosol particles with the same hygroscopic growth factor but different dry diameters enables the simultaneous determination of a_w and σ_{lv} as a function of solute concentration (see Methods and Supplementary Note 1). By applying the DKA approach to high precision measurement data from hygroscopic tandem differential mobility analyser (HTDMA) experiments[9] (see Methods), we obtained consistent and robust estimates for a_w and σ_{lv} of aqueous AS nanoparticles with molalities up to $b \sim 160\,mol\,kg^{-1}$ (solute mass fractions up to $x_s \sim 0.96$) (Fig. 2). The DKA results agree well with literature data in the previously accessible range of concentrations and enable accurate model calculations of the hygroscopic growth of highly concentrated AS nanoparticles (purple line in Fig. 1b); for DKA results of NaCl nanoparticles see Supplementary Fig. 1.

Measured and predicted phase transitions and equilibria. For model predictions of the DRH and ERH (efflorescence relative humidity), we calculated solute activity (a_s) and obtained the interfacial energy of the salt in its saturated aqueous solution upon deliquescence (σ_{sl}) and the interfacial energy of salt embryos (γ_{sl}) in highly supersaturated aqueous solution upon efflorescence based on the DKA-derived a_w and σ_{lv} (Supplementary Notes 2,3). With this approach, we are able to determine σ_{sl} and γ_{sl} at one particular diameter and then apply them for predictions over the entire size range of 6–60 nm (see Methods). As shown in Fig. 1c,d, the DKA-based thermodynamic data allow quantifying and reconciling the contrasting size dependencies in the relative humidity thresholds of the deliquescence and efflorescence transitions for both AS and NaCl nanoparticles. The experimental DRH values observed for NaCl and AS nanoparticles are in a good agreement with our Köhler-Ostwald-Freundlich model[15] using DKA data (solid lines in Fig. 1c) but not with the modelling approach neglecting the effect of particle size on solubility (dashed lines in Fig. 1c). The solute molality on deliquescence (b^*) represents the size-dependent water solubility of nanoparticles. It is much higher than the solubility of bulk material (b_{bulk}^*) and agrees well with the Ostwald-Freundlich model prediction (Fig. 1e). Owing to a lack of reliable a_s and σ_{sl} data, previous studies failed to reproduce the size-dependent solubility of AS, and therefore, were not able to explain the different size dependence of DRH for AS and NaCl[6,7].

The observed ERH values also agree very well with our predictions using DKA data (Fig. 1d) in a model combining the Köhler equation and classical nucleation theory[16,17] (see Methods). The solute molality upon efflorescence (b_e) represents the threshold concentration triggering solute nucleation and liquid–solid phase separation. It is not sensitive to particle size for NaCl, where a 30% increase in b_e was sufficient to maintain the same nucleation rate despite a 1,000-fold volume reduction between 60-nm and 6-nm particles (Fig. 3a and red diamonds in Fig. 1f). In contrast, an about 12-fold increase in b_e was required to trigger the nucleation and phase separation when going from 60-nm to 6-nm AS particles (Fig. 3b and blue circles in Fig. 1f). The different behaviour of NaCl and AS can be attributed largely to different relations between solute activity and concentration, that is, for the same change of activity, a stronger increase in molality is required for AS than for NaCl (Supplementary Fig. 2).

It has been shown that water activity rather than molality is the determinant for the homogenous nucleation of ice in solutions[18]. Similarly, our results demonstrate that solute nucleation and phase separation are determined by solute activity, implying that the non-ideality of solution properties become vital for the calculation of nucleation rates and understanding of phase transitions, especially for nanodroplets (Fig. 3). Indeed, the weaker size dependence of the threshold relative humidity (DRH, ERH) of AS is a consequence of its stronger size dependence of the threshold solute concentration (b^*, b_e) compared with NaCl (Supplementary Fig. 3).

The existence of metastable AS droplets with molalities up to $\sim 380\,mol\,kg^{-1}$ (AS:H_2O molar ratio ~7:1) upon efflorescence (Fig. 1f) provides new insight on the phase state of salt nanoparticles. Such a high solute-to-solvent ratio implies that the droplet is no longer a typical aqueous solution, but may be regarded as a 'molten' salt particle with a few water molecules as a

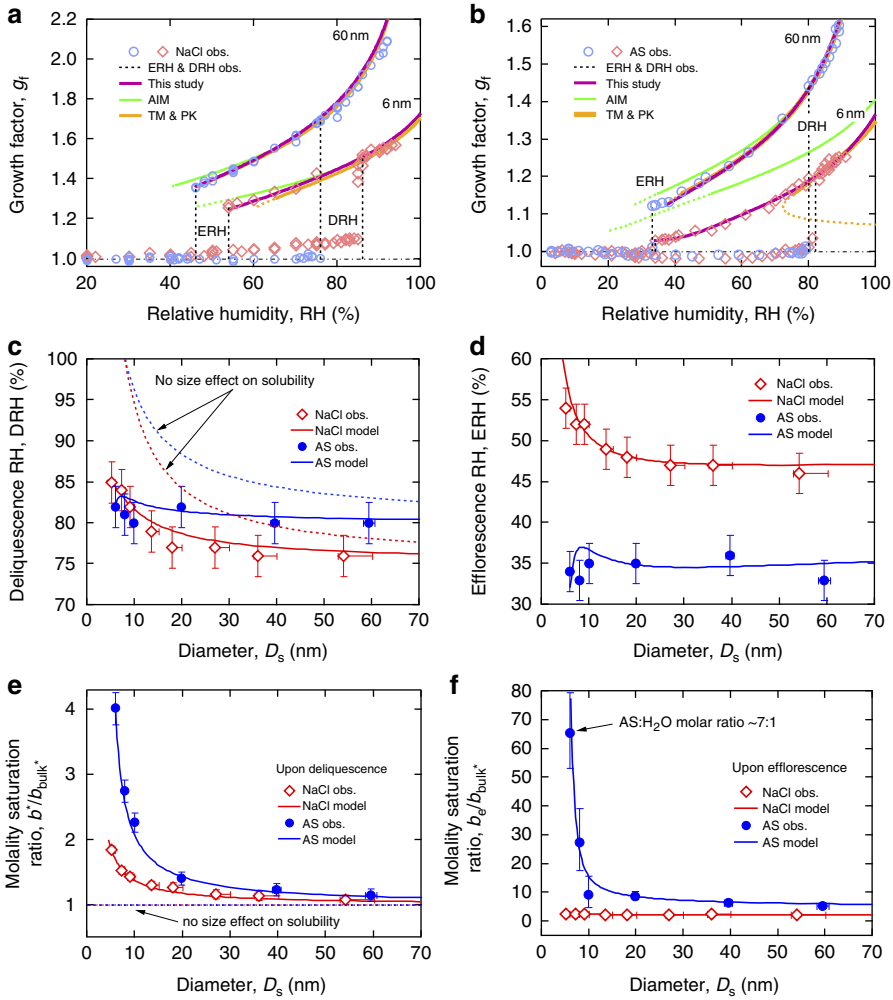

Figure 1 | Hygroscopic growth, deliquescence and efflorescence of nanoparticles. (**a**,**b**) Hygroscopic growth curves of sodium chloride (NaCl) and ammonium sulphate (AS). Growth factor data are taken from HTDMA experiments[8,9] for particles with dry diameters of 60 nm (blue circle) and 6 nm (red diamond). Köhler model curves are based on different thermodynamic data sets: in this study, purple line with DKA (Differential Köhler Analysis) derived data for AS and modified TM & SP (Tang-Munkelwitz[35,36] and Seinfeld-Pandis[37]) for NaCl; AIM (Aerosol Inorganics Model[38]), green line; TM & PK (Tang-Munkelwitz[35,36] and Pruppacher-Klett[39]) as in Biskos *et al.*[8,9], orange line (Supplementary Note 3). Dashed lines indicate extrapolation beyond validated concentration range. Size-dependent threshold values of relative humidity and solute saturation ratio on deliquescence (**c**,**e**) and efflorescence (**d**,**f**). Saturation ratios refer to bulk water solubility expressed in solute molality (b_{bulk}^*). Model curves were obtained by combination of the Köhler equation with the Ostwald–Freundlich equation for deliquescence and with classical nucleation theory for efflorescence. Dashed lines indicate model predictions without consideration of size-dependent solubility. Error bars are estimated by considering measurement uncertainties.

'solute' or 'impurity' (here 'molten' does not imply a high melting point). By further reducing particle size, we expect an increase in the AS mole fraction, such that the particle ultimately becomes a pure molten salt at ambient temperature. This is also supported by the fact that the interfacial energy σ_{lv} retrieved here at a temperature $T = 298\,K$ approaches a value of $0.182\,N\,m^{-1}$ (Fig. 2b), which is consistent with the value of $0.185\,N\,m^{-1}$ predicted for a molten AS at the same temperature[19].

Size effects on phase transitions. Although the Kelvin effect is commonly considered for liquid-vapour equilibrium and phase partitioning, size effects on the liquid-solid equilibrium upon phase transitions have been rarely taken into account in atmospheric thermodynamic and kinetic models. On the basis of the above results, we propose to include the particle dry diameter (D_s) as the third dimension in the liquid–solid equilibrium phase diagrams of aerosol particles. Figure 4a shows such a 3-D phase diagram for the AS-water system. In Fig. 4a, the surfaces represent the equilibrium between liquid and crystalline phases. It is estimated from polynomial fitting to literature data (solid circles). A slice on the surface at $D_s^{-1} = 0$ ($D_s \to \infty$) equals the traditional T-x_s diagram for bulk material as illustrated in Fig. 4b.

A slice on the surface at constant T provides a D_s^{-1}-x_s phase diagram showing the influence of particle size on equilibrium composition. As an example, Fig. 4c shows a D_s^{-1}-x_s slice at 215 K, which exhibits a similar pattern as the traditional T-x_s diagram in Fig. 4b. Figure 4d displays the D_s^{-1}-x_s diagram at 298 K, which contains the observed size-dependent solubility of AS particles reflecting the Ostwald–Freundlich effect[15]. Note that, at this temperature, the ice phase does not exist. Extrapolation of the experimental data for aqueous AS to $x_s = 1$ leads to a critical melting diameter of ~4 nm, that is, pure AS particles below this size are expected to be in a liquid state at 298 K.

Finally, a slice at constant x_s gives a T-D_s^{-1} phase diagram showing the effect of particle size on phase transition temperature (Fig. 4e). For example, in a system with an AS mass fraction of $x_s = 0.63$, the characteristic temperature for complete dissolution

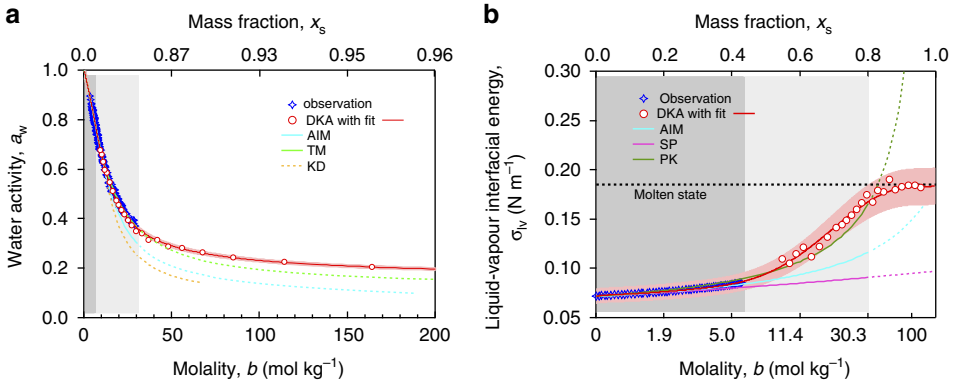

Figure 2 | Concentration-dependent thermodynamic properties of ammonium sulphate solution. (**a**,**b**) Water activity (a_w, on a mole fraction basis) and liquid-vapour interfacial energy (σ_{lv}) are plotted against solute molality (b) and mass fraction (x_s). The DKA-derived a_w and σ_{lv} (red open circles) are compared with observations (blue stars)[39,40], AIM (Aerosol Inorganic Model[38], blue line), and other parameterizations for a_w (TM = Tang-Munkelwitz[35], green line; KD = Kreidenweis[41], orange line) and σ_{lv} (PK = Pruppacher-Klett[39], dark green line; SP = Seinfeld-Pandis[37], purple line) (Supplementary Note 3). Dashed lines indicate extrapolation beyond validated concentration range. The equations for the best fit of DKA results (red lines) can be found in Supplementary Table 1. Red shaded areas indicate the uncertainties in the DKA retrieval, estimated by Monte Carlo analyses (Supplementary Note 1). The dark and light grey shaded areas mark the sub-saturated and saturated concentration with respect to bulk solution and supersaturated concentration before efflorescence of supermicrometre droplets, respectively. The white area marks the highly supersaturated concentration where the a_w data are not available in the literature.

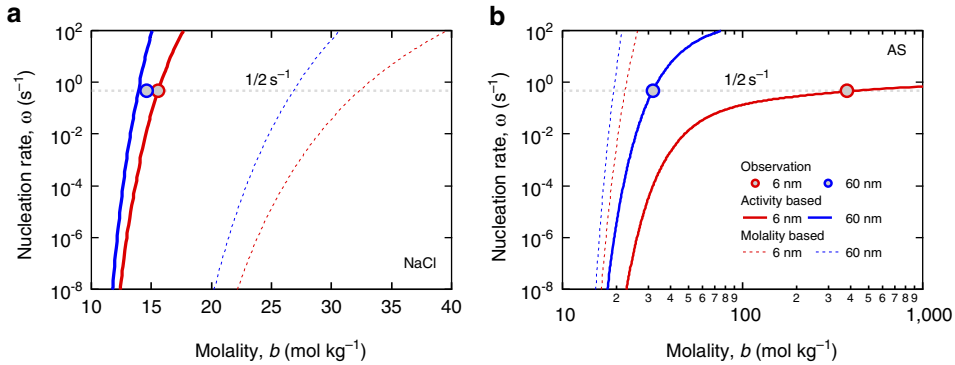

Figure 3 | Homogeneous nucleation rate as a function of solute molality. (**a**) Sodium chloride (NaCl) and (**b**) ammonium sulphate (AS). The nucleation rates (ω) are calculated from solute activity (thick lines) and concentration (thin dashed lines) at selected particle sizes (6 and 60 nm). Grey dashed line corresponds to ω of 0.5 s^{-1}, at which at least one nucleation event is triggered during the expected induction time interval (t_i and $\omega t_i = 1$). Here, t_i is estimated as 2 s according to the residence time in the HTDMA experiments[9]. The circles represent the observed nucleation (efflorescence) concentrations.

decreases from ~470 K for bulk material to ~298 K for 10-nm particles. At $x_s = 0$ or 1, the diagram becomes a T-D_s^{-1} diagram for a pure substance, reflecting the Gibbs–Thomson effect[20]. Related effects of particle size on melting, freezing and glass transitions have been reported and quantified for a wide range of materials such as water, organic compounds and metals[21–23] (Supplementary Fig. 4). Our results demonstrate that similar effects and formalisms also apply to other phase transition processes and mixed systems, such as liquid–solid phase separation in salt-water droplets. The size-dependent phase transition temperature and increased solubility of nanoparticles reflect a tendency of smaller particles for staying in liquid and mixed phase compared with bulk materials (Supplementary Fig. 5). This may partly explain the unresolved size-dependent morphology of organic-AS particles, that is, smaller particles are internally mixed while larger particles adopt a de-mixed partially engulfed structure[10].

Discussion

According to the size effects outlined above, aerosol particles of identical chemical composition may coexist in different states in the atmosphere depending on particle diameter. Thus, we are interested in the critical diameter ($D_{s,c}$) below which aerosol particles are expected to be liquid and well-mixed at ambient temperature. Using T-D_s^{-1} diagrams like Fig. 4e for particles with different chemical composition (Supplementary Fig. 6), we obtained critical dry diameters as a function of bulk phase transition temperature (T_{bulk}). As shown in Fig. 5, all data for aqueous AS and NaCl particles available at 298 K converge onto a compact near-linear correlation of $1/D_{s,c}$ versus T_{bulk}. The glass transition of low chain length polystyrene[22] as the only organic reference material (with low molecular weight) for which similar substrate-free data are currently available falls onto the same correlation line. These findings suggest that the influence of particle size on the liquefaction of substances is related to bulk phase transition temperature in a similar way for different salts as well as organic compounds, implying a close relationship between interfacial energy and the enthalpy of phase transition similar to the Turnbull relation[24] (see Supplementary Fig. 7 and Supplementary Discussion for more details).

Chamber experiments with pine emissions-derived secondary organic aerosol (SOA) as well as field measurements of

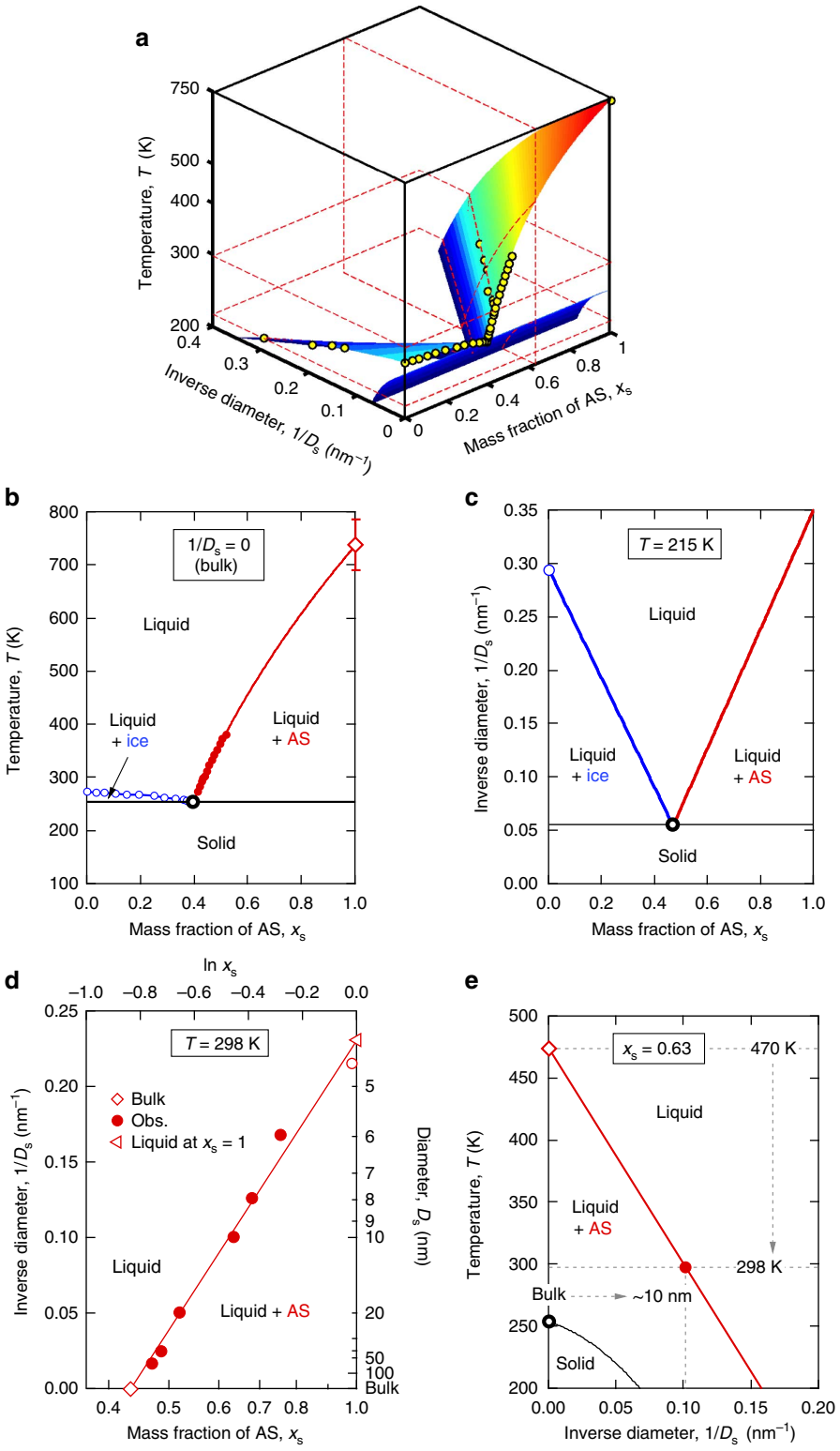

Figure 4 | Liquid–solid equilibrium phase diagrams for the ammonium sulphate—water system. (**a**) 3D phase diagrams in the coordinates of inverse diameter $1/D_s$, temperature T and ammonium sulphate (AS) mass fraction x_s. The solid circles represent the available data of bulk phase diagram of aqueous AS solution[42], size-dependent melting temperature of ice[23] and solubility of AS. The surfaces, coloured by the corresponding temperature, are estimated from polynomial fitting, showing the equilibrium between liquid and crystalline phases. The dashed planes illustrate the following slices. (**b**) The T-x_s phase diagram for bulk solution. The temperature-dependent phase separation of aqueous AS bulk solution (red line) is constrained by the melting temperature of AS at $x_s = 1$ (open diamond). The error bar shows the uncertainty of AS melting temperature according to close-cell measurements[43]. The D_s^{-1}-x_s phase diagram at 215 K (**c**) and at 298 K (**d**). In (**d**), the solid circles represent the observations for nano-sized droplets. The open diamond is the bulk solubility and the open circle is predicted by the DKA-constrained solute activity. The critical melting diameter (open triangle) is obtained by linear extrapolation to $x_s = 1$ (molten state). (**e**) The T-D_s^{-1} phase diagram at $x_s = 0.63$. The black open circle represents the eutectic point for bulk solution (also in **b** and **c**). The black line shows the size dependence of eutectic points.

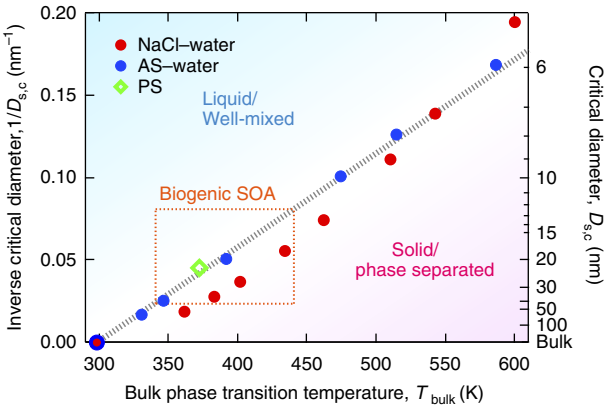

Figure 5 | Dependence of critical diameter on bulk phase transition temperature. Inverse critical diameters of liquefaction at 298 K ($D_{s,c}^{-1}$) are plotted against bulk phase transition temperatures (T_{bulk}) for aqueous ammonium sulphate (AS, blue solid circle), aqueous sodium chloride (NaCl, red solid circle) and low chain length polystyrene (PS, green open diamond)[22]. The data points are observations and the dotted line is a linear fit to all data through the point of [298 K, $D_s^{-1}=0$]. The orange dashed line bounded area indicates the parameter range estimated for atmospheric biogenic secondary organic aerosol (SOA).

atmospheric biogenic SOA indicate a change of particle phase state at ~20–30 nm (refs 3,25), suggesting that particles below this limit are in the liquid-like state. This observation appears consistent with a critical diameter around ~20 nm (12–40 nm), which can be derived from the estimated bulk melting temperatures of individual functionalized acids found in biogenic SOA (~340–440 K, orange dashed line bounded area in Fig. 5, see Supplementary Note 4)[2]. This consistency increases confidence in the similarity of T_{bulk}-$D_{s,c}$ relations. SOA particles usually consist of mixtures of multiple compounds, which reduces the bulk melting temperature[26], thus increasing the critical diameter and implying that SOA particles in the nucleation mode are very likely always liquid (of potentially high viscosity). The liquid-to-solid transition of SOA particles observed at ~20–30 nm was suggested to be a glass transition[3,25], for which the transition temperature is usually by a factor of ~0.7 lower than for melting[2]. Explaining the observed transition would thus require a fairly high bulk glass transition temperature (~370 K), suggesting that the SOA particles may contain oligomers or polymers, in agreement with independent observations[27].

The methods and results presented in this study advance the understanding and challenge the traditional modelling of atmospheric aerosol phase state and processing. The size effects on the phase states may have important implications for a number of atmospheric interfacial and condensed phase processes such as nucleation, water/gas uptake, polymerization and heterogeneous reactions[2,27–29]. The combination of the DKA method and tandem differential mobility analyser technique can be used to study the thermodynamic properties of nanoparticles from a wide range of materials and enables substrate-free experimental investigation of nanoparticles not only on humidification and drying but also with regard to other types of conditioning, for example, exposure to organic solvents, heat treatment and volatilization[30,31]. Thus, the scientific approach presented here may be useful for nanoparticle studies in various fields, including the environmental, biomedical and materials sciences[20,32].

Methods

HTDMA experiments. Our analysis is based on the Harvard hygroscopic tandem differential mobility analyser (HTDMA) measurements[8,9], where a mono-disperse dry particle fraction of dry diameter D_s is selected by the first DMA, equilibrated to a defined relative humidity (equivalent to water vapour saturation ratio s_w = RH/100%) and finally goes through a second DMA for the determination of the humidified size distribution. The HTDMA results were usually reported in the form of the growth factor g_f as a function of s_w at each D_s. Details of shape factor correction of HTDMA data can be found in Supplementary Note 1. Data from the efflorescence mode experiments (containing the most concentrated droplet solutions) are adopted for the DKA analysis.

Differential Köhler analysis (DKA). The theoretical basis of the DKA method is the Köhler equation[33], which describes the equilibrium s_w over a spherical droplet as a function of a_w, σ_{lv} and the droplet size D_{sol}

$$s_w = a_w \exp\left(\frac{4\sigma_{lv}v_w}{RTD_{sol}}\right) = a_w \exp\left(\frac{4\sigma_{lv}v_w}{RTD_s g_f}\right) \quad (1)$$

where v_w is the partial molar volume of water (Supplementary Note 1), R is the universal gas constant and T is temperature. D_{sol} in equation (1) is often replaced by the product of D_s and g_f, in which D_s is the dry diameter of spherical solute particles and g_f is the particle geometrical diameter growth factor, that is, $g_f = D_{sol}/D_s$. As parameters s_w, D_s and g_f can be determined from the HTDMA measurements, σ_{lv} and a_w (considered as size-independent) become the only unknowns in equation (1). Note that σ_{lv} and a_w are both functions of g_f (g_f represents the solute concentration x_s, see Supplementary Note 1). For each x_s (or g_f), we need to construct at least two independent equations by performing HTDMA measurements at different D_s to realize the differential analysis as follows. Converting equation (1) into logarithmic form, we have

$$\ln s_w = \ln a_w(g_f) + \frac{A}{D_s}\sigma_{lv}(g_f) \quad (2)$$

where $A = 4v_w/(RTg_f)$. With measurements at two dry diameters D_{s1} and D_{s2}, we have

$$a_w = \frac{S_{w1}^{\left(\frac{D_{s1}}{D_{s1}-D_{s2}}\right)}}{S_{w2}^{\left(\frac{D_{s2}}{D_{s1}-D_{s2}}\right)}} \quad \text{and} \quad \sigma_{lv} = \left(\frac{A}{D_{s1}} - \frac{A}{D_{s2}}\right)^{-1}(\ln s_{w1} - \ln s_{w2}) \quad (3)$$

where s_{w1} and s_{w2} are measured at the same g_f but at D_{s1} and D_{s2}, respectively. When measurements at the same g_f are available for more than two initial particle dry diameters, a multiple regression was applied to all sizes resulting in a best estimate of a_w and σ_{lv}. More details about the DKA method can be found in Supplementary Note 1.

Modelling of deliquescence and efflorescence. Deliquescence of salt particle of dry diameter D_s happens when the ambient s_w equals the equilibrium s_w over a droplet of the wet diameter equal to D_s, and saturated with respect to crystalline salt particles of size D_s. The deliquescence concentration b^* was determined by the Ostwald–Freudlich equation[15] through corresponding deliquescence solute activity a_s^*

$$a_s^* = a_{s,bulk}^* \exp\frac{4\sigma_{sl}M_s}{m_i\rho_s RTD_s} \quad (4)$$

in which a_s^* is the solute activity in a solution saturated with respect to salt particles of diameter D_s, $a_{s,bulk}^*$ is the solute activity in saturated bulk solution, M_s is molar weight of solute, ρ_s is the density of solute and m_i is the stoichiometric number of dissociated ions. The σ_{sl} is determined to be 0.156 and 0.265 N m^{-1} for AS and NaCl, respectively (Supplementary Note 2). Substituting b^* into the Köhler equation (1) gives the DRH.

The efflorescence is predicted based on classical nucleation theory[16,17,34] along with the Köhler equation[33]. Given a Köhler curve, the volume of the droplet V_{sol} and corresponding b at each point can be easily determined. Then we can calculate the nucleation rate ω at each point by[16]

$$\omega = JV_{sol} = V_{sol}K \exp\left(-\frac{4\left(\sum_j k_j\right)\alpha^2\gamma_{sl}^3}{27\Delta G_v^2 k_b T}\right) \quad (5)$$

where V_{sol} is the volume of the droplet, K is the pre-exponential factor, k_j and α are geometrical constants dependent on the morphology of the particular crystal, ΔG_v is the excess free energy of solute per unit volume in the crystalline phase over that in solution, k_b is the Boltzmann constant. We assumed that the formation of a single critical-sized nucleus is sufficient to initiate the crystallization of the entire droplet and trigger the efflorescence. Then ERH and b_e can be determined from the point where $\omega t_i = 1$ ($t_i = 2$ s is the induction time interval for the investigated system[9]) (Fig. 3). We performed model predictions of DRH and ERH over the entire size range of 6–60 nm for AS and NaCl by this approach with σ_{sl} and γ_{sl} determined at one particular diameter (6 nm, Supplementary Note 2).

References

1. Martin, S. T. Phase transitions of aqueous atmospheric particles. *Chem. Rev.* **100,** 3403–3454 (2000).
2. Koop, T., Bookhold, J., Shiraiwa, M. & Poschl, U. Glass transition and phase state of organic compounds: dependency on molecular properties and implications for secondary organic aerosols in the atmosphere. *Phys. Chem. Chem. Phys.* **13,** 19238–19255 (2011).
3. Virtanen, A. *et al.* An amorphous solid state of biogenic secondary organic aerosol particles. *Nature* **467,** 824–827 (2010).
4. Pöschl, U. Atmospheric aerosols: composition, transformation, climate and health effects. *Angew. Chem. Int. Ed.* **44,** 7520–7540 (2005).
5. Krieger, U. K., Marcolli, C. & Reid, J. P. Exploring the complexity of aerosol particle properties and processes using single particle techniques. *Chem. Soc. Rev.* **41,** 6631–6662 (2012).
6. Russell, L. M. & Ming, Y. Deliquescence of small particles. *J. Chem. Phys.* **116,** 311–321 (2002).
7. Orr, Jr C., Hurd, F. K. & Corbett, W. J. Aerosol size and relative humidity. *J. Colloid Sci.* **13,** 472–482 (1958).
8. Biskos, G., Russell, L. M., Buseck, P. R. & Martin, S. T. Nanosize effect on the hygroscopic growth factor of aerosol particles. *Geophys. Res. Lett.* **33,** L07801 (2006).
9. Biskos, G., Paulsen, D., Russell, L. M., Buseck, P. R. & Martin, S. T. Prompt deliquescence and efflorescence of aerosol nanoparticles. *Atmos. Chem. Phys.* **6,** 4633–4642 (2006).
10. Veghte, D. P., Altaf, M. B. & Freedman, M. A. Size dependence of the structure of organic aerosol. *J. Am. Chem. Soc.* **135,** 16046–16049 (2013).
11. Damson, A. W. & Gast, A. P. *Physical Chemistry of Surfaces*, 6th edn (John Wiley & Sons, Inc., 1997).
12. Vicente, C., Yao, W., Maris, H. J. & Seidel, G. M. Surface tension of liquid ^{4}He as measured using the vibration modes of a levitated drop. *Phys. Rev. B* **66,** 214504 (2002).
13. Tang, I. N., Munkelwitz, H. R. & Wang, N. Water activity measurements with single suspended droplets: The NaCl-H_2O and KCl-H_2O systems. *J. Colloid Interf. Sci.* **114,** 409–415 (1986).
14. Chan, C. K., Liang, Z., Zheng, J., Clegg, S. L. & Brimblecombe, P. Thermodynamic properties of aqueous aerosols to high supersaturation: I-measurements of water activity of the system $Na^+ - Cl^- - NO_3^- - SO_4^{2-} - H_2O$ at ~298.15K. *Aerosol Sci. Tech.* **27,** 324–344 (1997).
15. Ostwald, W. Über die vermeintliche isomerie des roten und gelben Quecksilbersoxyds und die Oberflächenspannung fester Körper. *Z. Phys. Chem.* **34,** 495–503 (1900).
16. Cohen, M. D., Flagan, R. C. & Seinfeld, J. H. Studies of concentrated electrolyte solutions using the electrodynamic balance. 3. Solute nucleation. *J. Phys. Chem.* **91,** 4583–4590 (1987).
17. Gao, Y., Chen, S. B. & Yu, L. E. Efflorescence relative humidity of airborne sodium chloride particles: A theoretical investigation. *Atmos. Environ.* **41,** 2019–2023 (2007).
18. Koop, T., Luo, B., Tsias, A. & Peter, T. Water activity as the determinant for homogeneous ice nucleation in aqueous solutions. *Nature* **406,** 611–614 (2000).
19. Dutcher, C. S., Wexler, A. S. & Clegg, S. L. Surface tensions of inorganic multicomponent aqueous electrolyte solutions and melts. *J. Phys. Chem. A* **114,** 12216–12230 (2010).
20. Alcoutlabi, M. & McKenna, G. B. Effects of confinement on material behaviour at the nanometre size scale.. *J. Phys.: Condens. Matter* **17,** R461 (2005).
21. Couchman, P. R. & Jesser, W. A. Thermodynamic theory of size dependence of melting temperature in metals. *Nature* **269,** 481–483 (1977).
22. Forrest, J. A. & Mattsson, J. Reductions of the glass transition temperature in thin polymer films: Probing the length scale of cooperative dynamics. *Phys. Rev. E* **61,** R53–R56 (2000).
23. Pan, D., Liu, L.-M., Slater, B., Michaelides, A. & Wang, E. Melting the ice: on the relation between melting temperature and size for nanoscale ice crystals. *ACS Nano* **5,** 4562–4569 (2011).
24. Turnbull, D. Formation of crystal nuclei in liquid metals. *J. Appl. Phys.* **21,** 1022–1028 (1950).
25. Virtanen, A. *et al.* Bounce behavior of freshly nucleated biogenic secondary organic aerosol particles. *Atmos. Chem. Phys.* **11,** 8759–8766 (2011).
26. Marcolli, C., Luo, B. & Peter, T. Mixing of the organic aerosol fractions: liquids as the thermodynamically stable phases. *J. Phys. Chem. A* **108,** 2216–2224 (2004).
27. Kalberer, M. *et al.* Identification of polymers as major components of atmospheric organic aerosols. *Science* **303,** 1659–1662 (2004).
28. Murray, B. J. *et al.* Heterogeneous nucleation of ice particles on glassy aerosols under cirrus conditions. *Nat. Geosci.* **3,** 233–237 (2010).
29. Shiraiwa, M., Ammann, M., Koop, T. & Poschl, U. Gas uptake and chemical aging of semisolid organic aerosol particles. *Proc. Natl Acad. Sci. USA* **108,** 11003–11008 (2011).
30. Joutsensaari, J., Vaattovaara, P., Vesterinen, M., Hämeri, K. & Laaksonen, A. A novel tandem differential mobility analyzer with organic vapor treatment of aerosol particles. *Atmos. Chem. Phys.* **1,** 51–60 (2001).
31. Cheng, Y. F. *et al.* Size-resolved measurement of the mixing state of soot in the megacity Beijing, China: diurnal cycle, aging and parameterization. *Atmos. Chem. Phys.* **12,** 4477–4491 (2012).
32. Rabinow, B. E. Nanosuspensions in drug delivery. *Nat. Rev. Drug Discov.* **3,** 785–796 (2004).
33. Köhler, H. The nucleus in and the growth of hygroscopic droplets. *Trans. Faraday Soc.* **32,** 1152–1161 (1936).
34. Gao, Y., Chen, S. B. & Yu, L. E. Efflorescence relative humidity for ammonium sulfate particles. *J. Phys. Chem. A* **110,** 7602–7608 (2006).
35. Tang, I. N. & Munkelwitz, H. R. Water activities, densities, and refractive indices of aqueous sulfates and sodium nitrate droplets of atmospheric importance. *J. Geophys. Res-Atmos.* **99,** 18801–18808 (1994).
36. Tang, I. N. Chemical and size effects of hygroscopic aerosols on light scattering coefficients. *J. Geophys. Res-Atmos.* **101,** 19245–19250 (1996).
37. Seinfeld, J. H. & Pandis, S. N. *Atmospheric Chemistry and Physics, from Air Pollution to Climate Change* (John Wiley, 2006).
38. Clegg, S. L., Brimblecombe, P. & Wexler, A. S. Thermodynamic Model of the System $H^+ - NH_4^+ - Na^+ - SO_4^{2-} - NO_3^- - Cl^- - H_2O$ at 298.15K. *J. Phys. Chem. A* **102,** 2155–2171 (1998).
39. Pruppacher, H. R. & Klett, J. D. *Microphysics of clouds and precipitation* (Kluwer Academic Publishers, 1997).
40. Clegg, S. L., Ho, S. S., Chan, C. K. & Brimblecombe, P. Thermodynamic properties of aqueous $(NH_4)_2SO_4$ to high supersaturation as a function of temperature. *J. Chem. Eng. Data* **40,** 1079–1090 (1995).
41. Kreidenweis, S. M. *et al.* Water activity and activation diameters from hygroscopicity data-Part I: Theory and application to inorganic salts. *Atmos. Chem. Phys.* **5,** 1357–1370 (2005).
42. Xu, J., Imre, D., McGraw, R. & Tang, I. Ammonium sulfate: equilibrium and metastability phase diagrams from 40 to −50°C. *J. Phys. Chem. B* **102,** 7462–7469 (1998).
43. Kendall, J. & Davidson, A. W. The melting point of ammonium sulfate. *J. Ind. Eng. Chem.* **13,** 303–304 (1921).

Acknowledgements

This study was supported by the Max Planck Society (MPG), National Natural Science Foundation of China (41330635), the EU project PEGASOS (265148), Russian Foundation for Basic research (12-05-00620-à), and RC 'Geomodel' of St Petersburg State University.

Author contributions

Y.C. and H.S. designed and performed the study. T.K., E.M. and U.P. discussed the results, interpretation and implications and commented on the manuscript at all stages. Y.C. and H.S. wrote the supplement. Y.C., H.S. and U.P. wrote the manuscript with inputs from all the co-authors.

Additional information

Supplementary Information accompanies this paper at http://www.nature.com/naturecommunications

Competing financial interests: The authors declare no competing financial interests.

Reprints and permission information is available online at http://npg.nature.com/reprintsandpermissions/

How to cite this article: Cheng, Y. *et al.* Size dependence of phase transitions in aerosol nanoparticles. *Nat. Commun.* 6:5923 doi: 10.1038/ncomms6923 (2015).